nature communications

Article

https://doi.org/10.1038/s41467-025-63576-y

A biopiezocatalyst harnessing mechanical energy to enhance bioplastic production from CO_2 and organic carbon

Received: 12 March 2025

Accepted: 22 August 2025

Published online: 30 August 2025

Check for updates

Pier-Luc Tremblay[1,2,3], Mengying Xu[1], Muhammad Babur Joya[1], Yujie Wang[1], Chun He[1], Ziqiu Li[3], Lian Li[1,2], Kai Xu[4], Yujie Feng[5] & Tian Zhang[1,2,3]

The sustainable bioproduction of chemicals from CO_2 remains far from reaching its full potential. The productivity of autotrophic bioprocesses could benefit from harnessing ubiquitous mechanical energy sources, which are inaccessible for energizing bioproduction systems to this day. In this work, we develop a hybrid system where the efficient piezocatalyst zinc oxide (ZnO) harnesses mechanical vibration to stimulate the growth of the chemolithoautotrophic bacterium *Cupriavidus necator* and its production of the bioplastic polyhydroxybutyrate (PHB) from CO_2. Both ultrasonication and intense wave-like motion at least triple autotrophic PHB production with ZnO forming a cohesive aggregate with *C. necator* and transferring charges to its respiratory metabolism. The same ZnO-*C.necator* system doubles heterotrophic PHB synthesis from fructose, highlighting its extensive potential for multiple biosynthesis applications. The hybrid approach reported here provides a blueprint route for powering bioproduction from CO_2 or other substrates with widespread mechanical energy such as industrial vibrations and natural waves.

A considerable fraction of anthropogenic CO_2 emissions responsible for climate change comes from the usage of oil, coal, and gas. This includes the production of multicarbon commodity chemicals, fuels, and plastics, still mostly derived from fossil resources[1–3]. A promising alternative is industrial biotechnologies converting CO_2 or other C1 feedstocks to value-added products[4]. With these approaches, autotrophic microbes reduce CO_2 to synthesize multicarbon chemicals, both preventing greenhouse gases from entering the atmosphere and competing with CO_2-generating technologies[5,6].

Critical limitations are still impeding the widespread implementation of CO_2-based biosynthesis technologies, including low productivity and energetic inefficiency[7]. One of the reasons for these persistent hurdles is that autotrophic microbes evolved over time to maximize their growth and dispersion, while their capacity for harvesting energy efficiently to drive biosynthesis processes was not prioritized[8,9]. A possible solution to solve these issues is to assist CO_2-fixing microbes in accessing energy sources usually inaccessible to them by developing hybrid abiotic-biological production systems[10–12]. So far, research in this area has mainly focused on particulate photocatalysts collecting solar energy and converting it to electrical or chemical energy, before transferring it to non-photosynthetic microbes for CO_2 bioconversion to valuable products[13–15]. While this strategy ends up mimicking natural photosynthesis, hybrid systems, with the right abiotic components, could be developed with other types of energy in mind such as mechanical energy, which is abundant but unattainable to autotrophic bioproduction processes.

Piezoelectric materials are non-centrosymmetric crystalline materials that convert mechanical energy into electrical energy[16,17].

[1]School of Chemistry, Chemical Engineering, and Life Science, Wuhan University of Technology, Wuhan, PR China. [2]Sanya Science and Education Innovation Park, Wuhan University of Technology, Sanya, PR China. [3]Institut WUT-AMU, Wuhan University of Technology, Wuhan, PR China. [4]Center for Materials Research and Analysis, Wuhan University of Technology, Wuhan, PR China. [5]State Key Laboratory of Urban-rural Water Resource and Environment, School of Environment, Harbin Institute of Technology, Harbin, PR China. e-mail: tzhang@whut.edu.cn

Under mechanical stress, atomic displacements within the crystal lattice of these materials separate positive and negative charge centers, leading to the generation of electric dipole moments, which bring about a piezoelectric potential at the macroscopic level[18]. It is this potential that drives the migration of free electrons (e^-) and holes (h^+) at the surface. Consequently, piezoelectric materials are researched for multiple applications, including the development of transducers, sensors, nanogenerators, and biomedical therapies, as well as for piezocatalysis through redox processes such as H_2 evolution, CO_2 reduction, pollutant degradation, and disinfection[19–23]. To date, piezoelectric materials have not been explored for energizing autotrophic bioproduction from CO_2 conversion. The only reported abiotic-biological systems including a piezocatalyst were described recently and focused on bacterial growth and wastewater denitrification[24,25].

Here, we assemble a biopiezocatalytic hybrid system comprising well-studied piezocatalytic ZnO nanosheets (NSs)[26] with the chemolithoautotrophic bacterium *Cupriavidus necator* H16, with the main objective of augmenting the production of the bioplastic polyhydroxybutyrate (PHB) from CO_2. In this system, ZnO converts mechanical energy, either from ultrasonic vibration or wave motion, into electrical energy, which is then transferred to *C. necator*, leading to an increase in intracellular reduced cofactors available for the bacterium's metabolism. Electric charges from ZnO are transferred to *C. necator* either as molecular hydrogen (H_2) or directly as e^- through flavins and c-type cytochromes released by the bacterium. The same hybrid system is also capable of augmenting PHB synthesis from fructose by providing additional reducing equivalents to the heterotrophic metabolism of *C. necator* via the mechanical stimulation of ZnO.

Results and discussion

The principle of the ZnO-*C. necator* biopiezocatalytic system

ZnO, a non-centrosymmetric wurtzite crystal, was selected as the piezocatalyst in this work because of extensive research demonstrating that it can generate, upon mechanical stimulation, e^- at a potential that would be suitable to enhance the metabolism of microbial cells (Fig. 1a, b, Supplementary Figs. 1, 2, and 3, Supplementary Discussion 1)[27–29]. For the biological component of the hybrid system, aerobic *C. necator*, which fixes CO_2 via the Calvin–Benson–Bassham (CBB) cycle, was chosen because it is a model strain for the autotrophic synthesis of PHB exhibiting good productivity towards this polymer[30,31]. In addition, several studies from our group showed that *C. necator* can acquire charges from the surface of (photo)catalytic particles by direct contact[10,32]. PHB itself is an important biodegradable and biocompatible product with an increasing market for applications in packaging, biomedical engineering, construction, textile, and so on[33].

Scanning electron micrograph (SEM) micrographs of the hybrid system under CO_2-fixing conditions showed that ZnO NSs aggregated with *C. necator* cells with close physical contacts between the abiotic and biological components (Fig. 1c, Supplementary Fig. 4). The energy-dispersive X-ray spectroscopy (EDS) analysis confirmed the widespread distribution within the aggregate of Zn from ZnO only and O from both ZnO and the surface of *C. necator* (Fig. 1d). Next, we examined the local piezoelectric response at the surface of ZnO-*C. necator* by piezoresponse force microscopy (PFM) (Fig. 1e). From this technique, a distinctive butterfly-shaped amplitude curve and a PFM hysteresis loop exhibiting a phase angle change of ca. 180 °, when the DC voltage was reversed from −10 to 10 V, were indicative of a complete ferroelectric polarization switching (Fig. 1f). This observation highlights the generation of a piezoelectric potential when the conductive tip of the atomic force microscope (AFM) was scanning the ZnO-*C.necator* aggregate.

We then examined interfacial charge transfer between ZnO and *C. necator*. First, the transient piezoelectric current response was measured by submitting the hybrid system to an on/off cycle of ultrasonication (US) at 96 W (Fig. 1g). Results confirmed that ZnO was mechanically stimulated. The higher piezoelectric current detected with the ZnO-*C. necator* couple, compared to ZnO only, suggested that charge carrier separation became more efficient in ZnO, possibly because of charge transfer to bacterial cells. This observation was supported by electrical impedance spectroscopy (EIS) and steady-state photoluminescence (PL) analyses (Fig. 1h, i). Nyquist plots derived from EIS data showed that mechanically stimulated ZnO had a lower charge transfer resistance (R_{ct}) when combined with *C. necator* cells. In the same vein, *C. necator* quenched PL from ZnO NS, probably because microbial cells accelerated charge transfer, which attenuated e^-/h^+ recombination in the piezocatalyst. Altogether, these results provide evidence that ZnO, upon mechanical stimulation, transfers charges to *C. necator*, which incidentally improves its piezocatalytic performance.

Bioplastic production from CO_2 and mechanical energy

To determine if ZnO NSs could serve as a charge donor for autotrophic PHB production, we added the piezocatalyst to a *C. necator* batch culture growing at 30 °C under a H_2:CO_2:O_2 atmosphere with overabundant CO_2 (Fig. 1a). We then stimulated ZnO NSs by US at 96 W for 1 h per day. To ensure good microbial growth and promote effective mass transfer from gas to the liquid phase, the culture was mildly agitated on a standard orbital shaker. A *C. necator* culture without ZnO and US produced only 282.15 ± 30 mg/L (n = 3 independent experiments) of PHB after 36 h with a yield of PHB from CO_2 ($Y_{PHB/CO2}$, g/g, %) of 11.0% (Fig. 2a, b, Supplementary Fig. 5). In this case, the only source of e^- for bacterial cells is H_2 provided in the gas phase. Cultivating *C. necator* either with ZnO in the absence of US or with periodic US but without ZnO had no significant impact on PHB production. In contrast, adding ZnO to *C. necator* and proceeding to daily US more than tripled PHB production to 1093.5 ± 47 mg/L (n = 3 independent experiments) with a $Y_{PHB/CO2}$ of 42.8% and a vibration energy-to-PHB efficiency of 2.42%, when considering a 1 L reactor (Fig. 2a, b, Supplementary Fig. 5, Supplementary Discussion 2). This result was obtained with 0.8 g/L of ZnO NS, yet amending the bacterial culture with only 0.1 g/L of the piezocatalyst nearly doubled PHB synthesis (Fig. 2c, d). From 0.1 to 0.8 g/L of ZnO, PHB production kept increasing, which showed that the positive impact on *C. necator* of the piezocatalyst correlated with its concentration. At 1 g/L of ZnO, the productivity of the biopiezocatalytic system plateaued. The replacement of ZnO NSs with 0.8 g/L of biocompatible, amorphous, and non-piezocatalytic SiO_2 particles did not increase PHB production upon US stimulation, indicating that the effect observed was specific to piezocatalytic ZnO NSs (Supplementary Fig. 6). Incubating the piezo-stimulated ZnO-*C. necator* system longer than 36 h resulted in a small diminution of the PHB concentration, which was likely due to *C. necator* cells starting to depolymerize the bioplastic upon starvation (Fig. 2a, c). Future work will aim to optimize the *C. necator* strain to ensure the stability of PHB bioproduction[34].

In a similar way to US, intense agitation at 200 rpm with a tilting shaker (referred to as wave motion from this point forward) instead of mild shaking with an orbital device stimulated ZnO and led to a multifold increase of PHB production after 36 h with a $Y_{PHB/CO2}$ of 40.1%, further demonstrating that our hybrid system can harness mechanical energy to convert CO_2 to biopolymer molecules (Fig. 2e, f, Supplementary Fig. 5 and Table 1). Intense tilting shaking generated a wave-like undulating movement likely capable of mechanically stimulating the ZnO piezocatalyst (Supplementary Fig. 7). Notably, a tracer experiment with ^{13}C-labeled bicarbonate amended to the growth medium confirmed that the ZnO-*C. necator* hybrid stimulated by US or wave was converting inorganic carbon into PHB (Supplementary Fig. 8). Furthermore, the PHB produced with our system had a molecular weight (M_w) of 2.3 MDa and a polydispersity index (PDI) of 2.1. For

https://doi.org/10.1038/s41467-025-63576-y

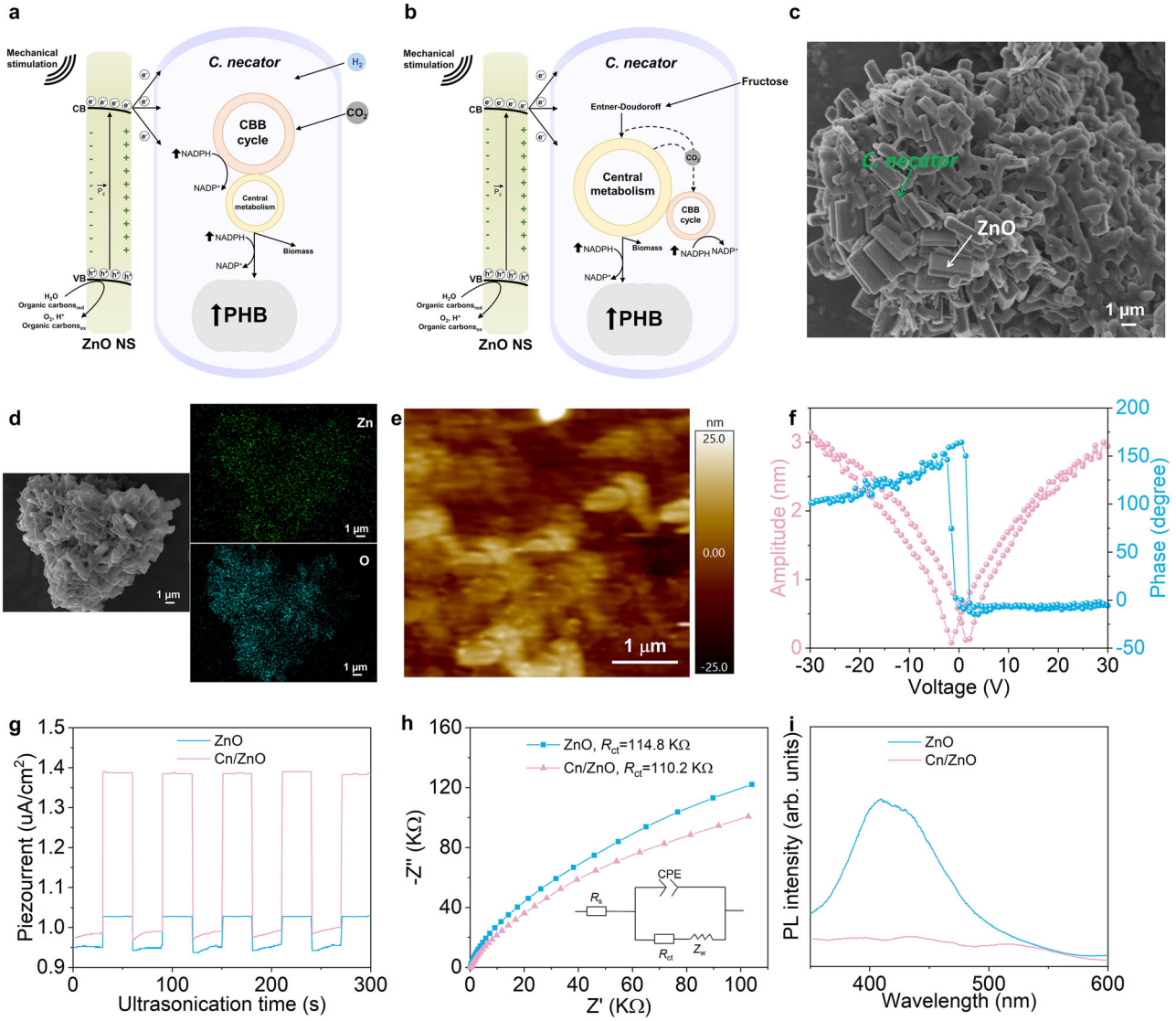

Fig. 1 | The ZnO-C. *necator* biopiezocatalytic system and demonstration of charge transfer between the piezocatalyst and the microbial cells. Principle of the **a** autotrophic and **b** heterotrophic piezocatalytic ZnO-*C. necator* hybrid system. Upon mechanical stimulation, ZnO transfers charges to *C. necator* grown with either atmospheric H_2 and CO_2 or fructose and provides complementary energy, leading to an increase in the intracellular NADPH/$NADP^+$ ratio and, ultimately, higher PHB production. **c** SEM micrograph, **d** Zn and O EDS maps of the hybrid system aggregate. **e** PFM topography, **f** piezoresponse butterfly-shaped curve, and hysteresis loop of ZnO-*C. necator*. **g** Transient piezoelectric current upon US (96W) of ZnO only and the ZnO-*C. necator* hybrid. **h** Nyquist plots and (**i**) PL spectra of mechanically-stimulated ZnO versus ZnO-*C. necator*. CBB Calvin-Bassham-Benson cycle, Cn *C. necator*. The inset on panel h is the proposed equivalent circuit with calculated charge transfer resistance (R_{ct}). Source data are provided as a Source Data file.

industrial usage, the M_w of PHB should be higher than 0.5 MDa, which was the case here, with a PDI that was also suitable for different applications[35].

Next, we measured the intracellular NADPH/$NADP^+$ cofactor ratio in bacterial cells of the hybrid system (Fig. 2g). The NADPH/$NADP^+$ ratio in *C. necator* increased to 0.82 ± 0.04 and 0.87 ± 0.02 ($n = 3$ independent experiments) when ZnO NSs in the batch culture were stimulated by US and wave motion, respectively. In comparison, *C. necator* cells without ZnO or with unstimulated ZnO had lower NADPH/$NADP^+$ ratios ranging from 0.61 to 0.69. Previous studies showed a similar phenomenon with illuminated photocatalytic particles augmenting the NADPH/$NADP^+$ ratio in *C. necator*[32,36]. During autotrophic PHB production, NADPH is essential for two key metabolic functions. First, NADPH provides the electrons and protons necessary for CO_2 reduction by the CBB cycle (Fig. 1a). Second, NADPH serves as the electron carrier for a core reaction of PHB synthesis from acetyl-CoA, which is the conversion by the NADPH-dependent acetoacetyl-CoA reductases PhaB1-3 of acetoacetyl-CoA into (R)-3-hydroxybutyryl-CoA[31,37]. The increase in NADPH in the biopiezocatalytic system is additional evidence that ZnO transferred charges to *C. necator*, which modulated the intracellular redox balance in a way that promoted PHB production from CO_2.

One factor to consider when working with ZnO and living bacteria is that the piezocatalyst is known to act as a disinfectant against a limited number of pathogens, via the generation of reactive oxygen species (ROS)[38,39]. Another possible stress in our system is the transient US that may damage bacterial cells. Live/dead staining results showed that these two factors did not negatively affect the viability of *C. necator*, which was $99.1 \pm 0.3\%$ and $98.6 \pm 1.0\%$ ($n = 3$ independent experiments) after 36 h of cultivation with ZnO stimulated by US or wave, respectively (Fig. 2h, Supplementary Fig. 9). A similar viability was observed for *C. necator* cultivated in the absence of both ZnO and US. These observations are not surprising considering that aerobic *C. necator* has several lines of defense against ROS and that it is one of the

https://doi.org/10.1038/s41467-025-63576-y

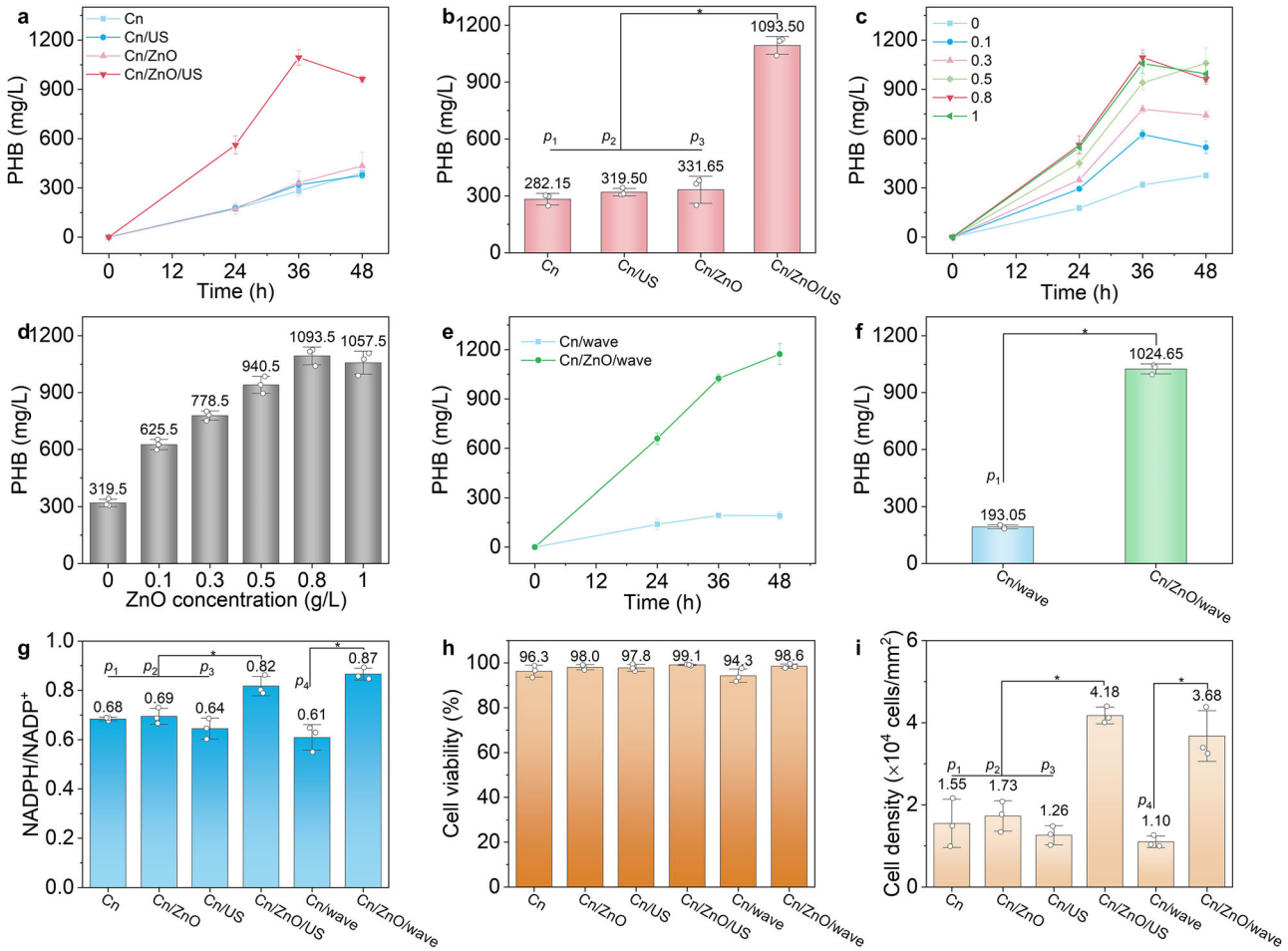

Fig. 2 | Autotrophic PHB production by the mechanically-stimulated ZnO-*C. necator* hybrid system. a The autotrophic PHB production time course over 48 h by ZnO-*C. necator* submitted to US at 96 W for 1 h per day. **b** Bar graph comparing the optimal PHB concentration observed with the US-stimulated hybrid system at 36 h versus PHB production by *C. necator* alone, submitted or not to US, or by ZnO-*C. necator* without US ($p_1 = 1.476 \times 10^{-5}$, $p_2 = 1.2360 \times 10^{-5}$, and $p_3 = 0.0001$). PHB production **c** time course curves and **d** bar graph of *C. necator* grown with 0 to 1 g/L ZnO NSs with US at 96 W for 1 h per day. **e** PHB production time course curves and **f** bar graph of *C. necator* alone or the ZnO-*C. necator* hybrid system submitted to intense wave motion via tilting agitation at 200 rpm ($p_1 = 8.5483 \times 10^{-8}$). **g** NADPH/NADP$^+$ ratios ($p_1 = 0.0044$, $p_2 = 0.0140$, $p_3 = 0.0065$, and $p_4 = 0.0015$), **h** viable cell percentages, and **i** cell densities after 36 h of autotrophic growth of the mechanically stimulated ZnO-C. *necator* hybrid system and the relevant controls ($p_1 = 0.0226$, $p_2 = 0.0078$, $p_3 = 0.0018$, and $p_4 = 0.0046$). Cn: *C. necator*. Data are mean ± s.d. ($n = 3$ independent experiments); two-tailed paired Student's *t*-test; $^*p \le 0.05$. Source data are provided as a Source Data file.

few robust microbes capable of growing with other semiconductor particles toxic to some bacteria[36,40,41].

Most importantly, cell counting after live/dead staining indicated that mechanically-stimulated ZnO NSs promoted *C. necator* growth (Fig. 2i). Compared to the control groups, cell densities, after 36 h in the autotrophic ZnO-*C. necator* system stimulated by US or wave motion, were several times higher. Thus, the coupling of the piezocatalyst with *C. necator* altered the intracellular redox balance and provided supplementary energy for bacterial growth and metabolism. This was further demonstrated by measuring the concentration of soluble proteins generated by *C. necator* when growing with piezo-stimulated ZnO NSs (Supplementary Fig. 10). The ZnO-*C. necator* hybrid produced 176.90 ± 7.60 mg/L and 164.54 ± 12.33 mg/L ($n = 3$ independent experiments) of soluble proteins when submitted to either daily US or wave motion, respectively. This was at least 1.8 times higher than the different controls examined. Besides providing additional evidence of the positive impact of ZnO NSs on the metabolism of *C. necator*, this result demonstrated that the biopiezocatalyst could synthesize another industrially relevant product. Soluble proteins from *C. necator* and other microbes, also known as single-cell proteins, are being developed as a substitute for animal and human nutrition[42].

Heterotrophic bioplastic production stimulated by ZnO nanosheets

In the next part of our study, we determined if piezo-stimulated ZnO could also increase heterotrophic PHB production from fructose (Figs. 1b, 3). With US for 1 h per day, the ZnO-*C. necator* hybrid system produced 8.20 ± 0.61 g/L PHB ($n = 3$ independent experiments) after 96 h with a vibration energy-to-PHB efficiency of 6.24% considering a 1 L reactor (Fig. 3a, b, Supplementary Discussion 2). In comparison, *C. necator* alone and *C. necator* with US or ZnO only produced 4.01 to 4.28 g/L PHB over the same period. Optimization of the heterotrophic process indicated that 96 W was the optimal US intensity and 0.5 g/L ZnO was the best piezocatalyst concentration (Fig. 3c, d, Supplementary Figs. 11 and 12). PHB production augmented gradually when increasing US intensity from 12 to 72 W and ZnO from 0.1 to 0.3 g/L. A higher US intensity of 120 W or a ZnO concentration above 0.5 g/L resulted in a lower PHB production compared to the optimal conditions. Many factors could be involved here, including the possible harmful effect of US at too high intensity on the bacterial cell integrity or the suboptimal interfacing between ZnO NSs and *C. necator* when ZnO is too concentrated.

When considering fructose consumption, the PHB yield ($Y_{PHB/fructose, \%}$) of the US-stimulated ZnO-*C. necator* system of 50.76%

https://doi.org/10.1038/s41467-025-63576-y

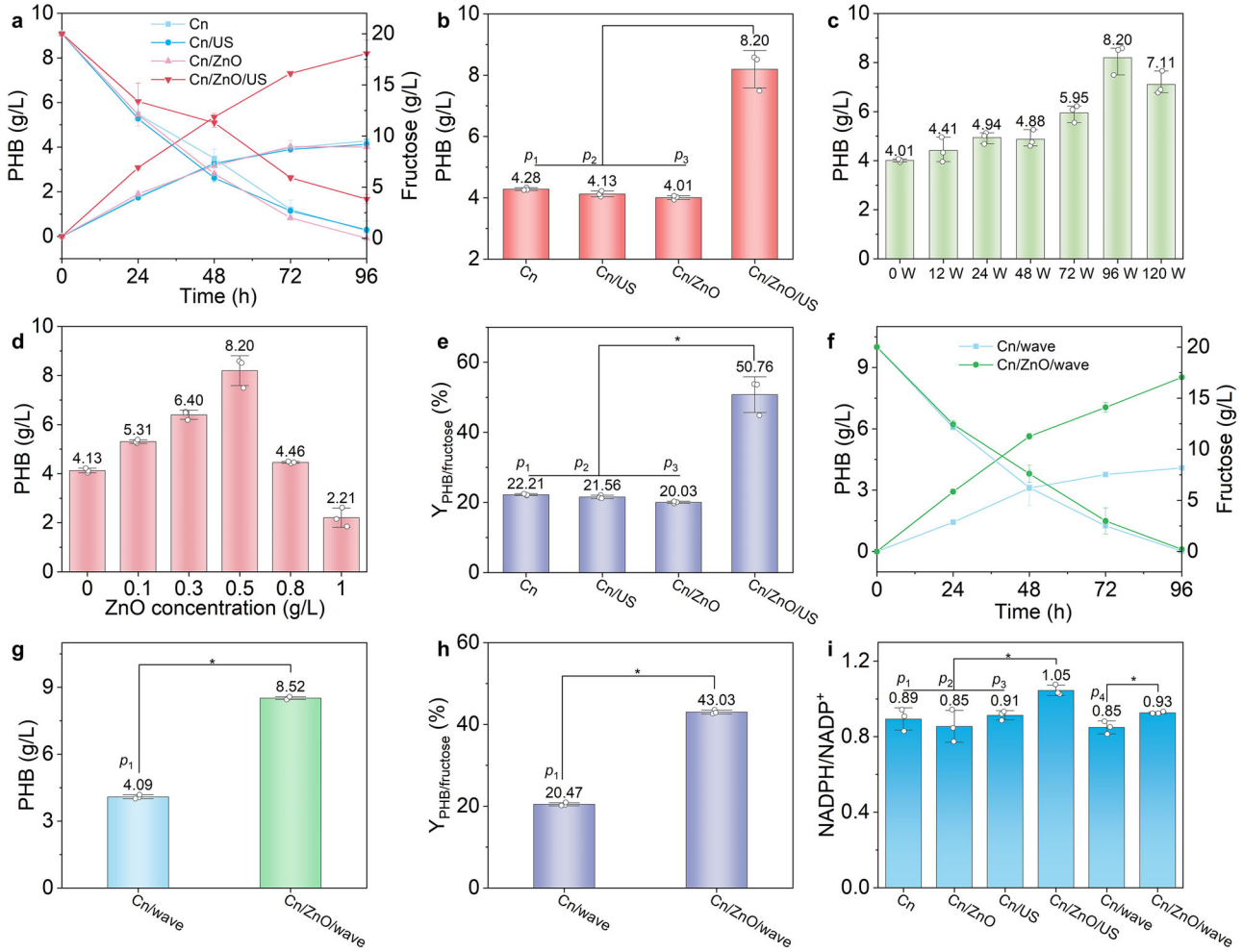

Fig. 3 | Heterotrophic PHB production from fructose by the hybrid ZnO-*C. necator* system stimulated with mechanical energy. a Heterotrophic PHB production and fructose consumption time course curves by ZnO-*C. necator* submitted to US at 96 W for 1 h per day. **b** Bar graph comparing the optimal PHB concentration observed with the US-stimulated hybrid system after 96 h of heterotrophic growth versus *C. necator* alone, submitted or not to US, or ZnO-*C. necator* without US ($p_1 = 0.0004$, $p_2 = 0.0003$, and $p_3 = 0.0003$). Heterotrophic PHB production bar graphs of the hybrid system cultivated **c** under different US intensities (with 0.5 g/L ZnO) or **d** with different ZnO NSs concentrations (US at 96 W for 1 h per day). **e** Yield of PHB from fructose ($Y_{PHB/fructose}$) bar graph for the US-stimulated ZnO-*C. necator* hybrid system and relevant controls ($p_1 = 0.0006$, $p_2 = 0.0006$, and $p_3 = 0.0005$). PHB production from fructose **f** time course curves and **g** bar graph of *C. necator* alone or the *C. necator*/ZnO hybrid system submitted to intense wave motion ($p_1 = 2.5123 \times 10^{-7}$). **h** $Y_{PHB/fructose}$ bar graph for the wave-stimulated ZnO-*C. necator* hybrid system. **i** NADPH/NADP$^+$ ratios bar graph ($p_1 = 0.0154$, $p_2 = 0.0209$, $p_3 = 0.0034$, and $p_4 = 0.0178$). Cn: *C. necator*. Data are mean ± s.d. ($n = 3$ independent experiments); two-tailed paired Student's *t*-test; $^*p \le 0.05$. Source data are provided as a Source Data file.

was at least 2.3 times higher than the three control groups (Fig. 3e). An important obstacle for bio-industrial heterotrophic PHB production is the considerable cost of organic carbon substrates[43]. A possible solution is to develop inexpensive approaches to augment PHB synthesis yield. Here, our results indicated that ZnO NSs can harness abundant mechanical energy to promote heterotrophic bioplastic production from fructose.

As with autotrophic production, intense wave motion at 200 rpm generated by a tilting shaker enhanced PHB synthesis from fructose in the presence of ZnO, with a biopolymer concentration at the end of the experiment of 8.52 ± 0.07 g/L ($n = 3$ independent experiments) (Fig. 3f, g). $Y_{PHB/fructose}$ was also significantly improved to 43.03%, further emphasizing that different mechanical stimuli can activate our hybrid system (Fig. 3h). Because of charge transfer from ZnO, the heterotrophic hybrid system stimulated by US or wave motion exhibited higher intracellular NADPH/NADP$^+$ ratios compared to all the control groups (Fig. 3i). In these growth conditions, a higher NADPH concentration is likely beneficial for the enzymatic conversion of acetyl-CoA to PHB. It is also possibly improving *C. necator*'s capacity for the recycling, by the NADPH-oxidizing CBB cycle, of CO_2 released during fructose oxidation (Fig. 1b)[32].

Lastly, ZnO, at an optimal concentration, US at 96 W for 1 h per day, or intense wave motion did not lessen heterotrophic cell viability compared to *C. necator* cultivated alone. This observation provides additional evidence of the robustness of this microbe in our biopiezocatalyst system (Fig. 4a, Supplementary Fig. 13). The live/dead staining results also showed that piezo-stimulated ZnO NSs promoted heterotrophic cell growth, which was augmented at least 1.6 times (Fig. 4b). This was accompanied by a production of soluble protein that was 1.3 to 1.5 times higher compared to controls after 36 h, reaching 506.43 ± 10.45 mg/L and 396.66 ± 29.88 mg/L ($n = 3$ independent experiments) when ZnO-*C. necator* grown with fructose was stimulated by daily US or wave motion (Supplementary Fig. 14). These observations are similar to the autotrophic hybrid system, where the intracellular redox balance, microbial growth, and metabolism were modulated by ZnO, leading to higher PHB and soluble protein production.

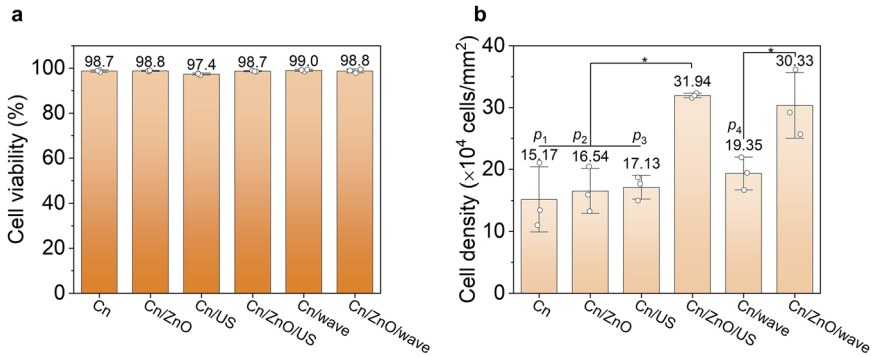

Fig. 4 | Cell viability and density in the biopiezocatalytic system producing bioplastic from fructose. a Viable cell percentages and **b** cell densities after 96 h of heterotrophic growth of the mechanically-stimulated ZnO-C. *necator* hybrid system and the relevant controls ($p_1 = 0.0053$, $p_2 = 0.0019$, $p_3 = 0.0002$, and $p_4 = 0.0326$). Cn: *C. necator*. Data are mean ± s.d. ($n = 3$ independent experiments); two-tailed paired Student's *t*-test; $^*p \le 0.05$. Source data are provided as a Source Data file.

H_2 and redox mediators released by *C. necator* involved in electron transfer from ZnO nanosheets

Next, we investigated how ZnO, upon mechanical stimulation, transferred charges and modulated the intracellular redox balance in *C. necator* in a way that stimulated growth and augmented biosynthesis. Determination of the energy band structure of the n-type ZnO NSs with a Tauc plot derived from UV-vis diffuse reflectance spectroscopy (DRS) data and a Mott–Schottky plot indicated that the conduction band edge (E_{cb}) of the piezocatalyst was −0.53 V while the valence band edge (E_{vb}) was 2.67 V (Fig. 5a, Supplementary Fig. 15). Because of the position of its E_{cb}, ZnO can, in theory, release charges that could drive the metabolism of *C. necator*, either as free e^- at a suitable redox potential or as H_2. As an aerobic microbe, *C. necator* possesses multiple cytochromes associated with its inner membrane[31,44]. *C. necator* also harbors other electron-transport (ET) proteins and molecules (e.g., Fe-S proteins, ubiquinone, flavin mononucleotide, flavin adenine dinucleotide) covering a wide range of midpoint potentials (− 0.45 to +0.35 V). This means that e^- from ZnO that could be transported across the distance between the piezocatalyst surface and the inner membrane of the microbe could readily be transferred to some of these elements. In addition, *C. necator* has two uptake hydrogenases, the membrane-bound (MBH) and the soluble hydrogenases (SH), and oxidizes H_2 readily.

Several studies reported that solid electron donors (SEDs), including photocatalytic materials and electrodes, reduced small electron shuttles such as H^+/H_2 that *C. necator* then oxidized via enzymatic activity to power its biosynthetic processes[10,32,36,45]. Because of its E_{cb} position, piezo-stimulated ZnO can generate H_2[27,28], including under physiological conditions (H^+/H_2, $E^{o\prime} = -0.41$ V). Our results confirmed that the ZnO NSs employed here evolved H_2 upon mechanical stimulation when incubated in cell-free spent medium from either autotrophic or heterotrophic cultures (Supplementary Fig. 16). In addition, a gene expression analysis of mechanically-stimulated autotrophic ZnO-*C. necator* showed that transcripts for the SH and MBH genes were highly abundant, indicating that the bacterium had the metabolic capacity to oxidize any H_2 molecules generated by ZnO (Supplementary Fig. 17, Supplementary Data 1).

However, mechanically stimulated ZnO NSs produced only limited quantities of H_2. After 1 h of US at 96 W, H_2 evolution by ZnO NSs in either autotrophic and heterotrophic cell-free spent media was 79.0-81.0 μmol/g (Supplementary Fig. 16). Assuming that H_2 evolution by ZnO NSs in the presence of metabolically-active *C. necator* cells was similar, it would be insufficient to account for the totality of the PHB production increases observed with the mechanically-stimulated ZnO-*C. necator* hybrid. This suggests that an alternative charge transfer mechanism between ZnO NSs and *C. necator* was involved.

A recent report mapping the photoelectrochemical current between a CdS-based semiconductor photoelectrode and *C. necator* proposed an ET mechanism independent of H_2 shuttling involving organic redox mediators, such as free flavins, released by the bacterium in the extracellular fraction[46]. Here, a cyclic voltammetry (CV) survey focusing on the supernatant of the ZnO-*C. necator* hybrid after 36 h of autotrophic growth indicated that similar redox molecules could be involved (Fig. 5b). Two sets of reduction and oxidation peaks, distinctive of reversible redox couples, were observed on the CV curve of the supernatant of the hybrid system stimulated by intense wave motion. In contrast, these peaks were absent from the ZnO-only control and less pronounced for the *C. necator*-only control. The first redox couple had a reduction and an oxidation peak of −0.14 and −0.10 V, respectively. This could be distinctive of free flavins, which have midpoint potentials usually between −0.12 and −0.3 V (Fig. 5c)[47]. The direct examination of the hybrid system's supernatant by fluorescence spectroscopy with an excitation wavelength of 425 nm confirmed the presence of flavin molecules emitting at ca. 525 nm (Fig. 5d,e)[48]. Interestingly, while the supernatant of *C. necator* grown alone contained flavins, fluorescence spectra showed that ZnO and mechanical stimulation increased the fraction of flavin molecules released by the microbial cells. This may indicate that bacteria were adapting to enhance their capacity for e^- uptake from the SED.

The second redox couple on the CV curve of the autotrophic hybrid system's supernatant was more pronounced and had a reduction and an oxidation peak of 0.23 and 0.35 V, respectively (Fig. 5b, c). In *C. necator*, cytochromes have midpoint potentials ranging from 0.05 to 0.418 V[49]. Thus, it is possible that this second redox couple corresponds to some of these cytochromes. Heme staining of the concentrated supernatant of the mechanically-stimulated hybrid system confirmed this hypothesis and indicated that the microbial cells released small cytochrome(s) of ca. 10 kDa in the extracellular fraction (Fig. 5f, Supplementary Figs. 18 and 19). Mass spectrometry identified two monoheme c-type cytochromes, H16_A1121 and H16_A3570, which are annotated as cytochrome c553 and cytochrome c551/c552, respectively. The key role of extracellular c-type cytochromes, including small ones, in ET between a SED and an electroactive microbe has been extensively characterized[50,51]. Our results suggest that H16_A1121 and H16_A3570 may have a similar function and contribute to charge transfer from ZnO. Notably, piezo-stimulated ZnO-*C. necator* transcriptomic results indicated that flavin synthesis-related genes, such as *ribD*, as well as the H16_A3570 gene, exhibited transcript abundances that were 1.5 and 1.7 times higher than the median gene expression, respectively (Supplementary Fig. 17, Supplementary Data 1).

Based on these observations, we propose a dual model where charges from ZnO NSs are transferred to autotrophic *C. necator* either

https://doi.org/10.1038/s41467-025-63576-y

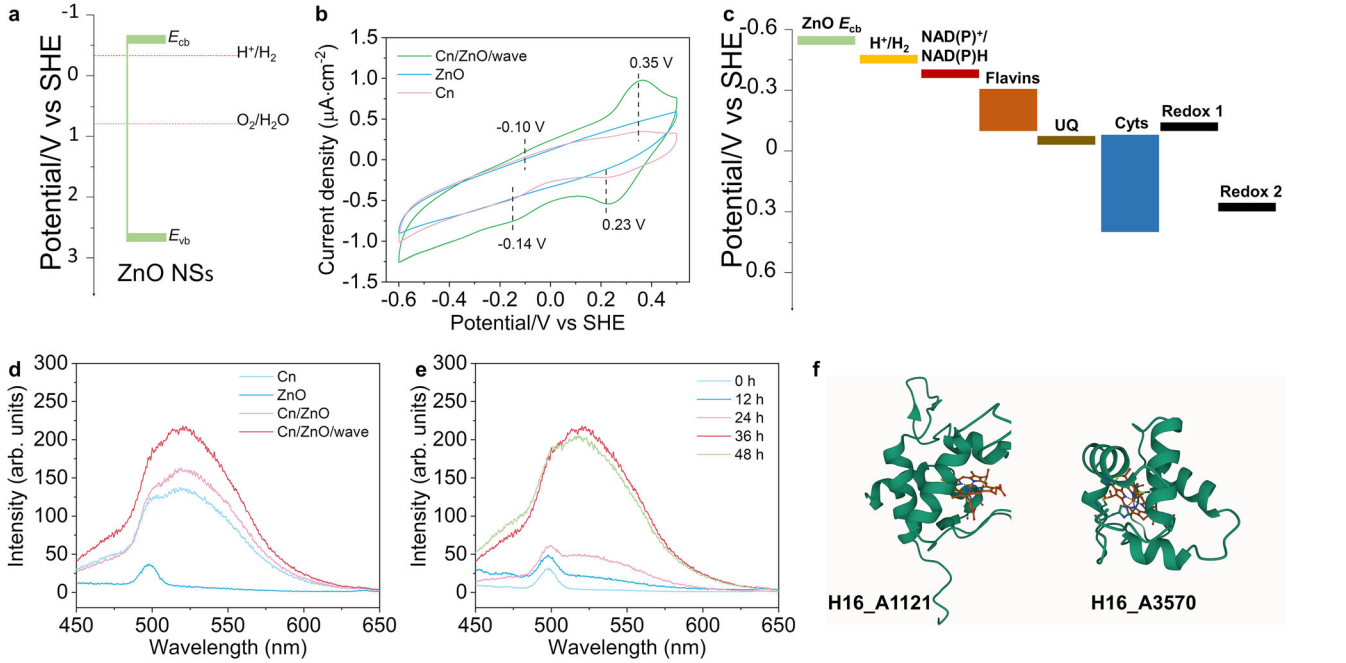

Fig. 5 | Components involved in charge transfer between piezo-stimulated ZnO nanosheets and *C. necator* cells. a Energy band diagram of ZnO NSs. **b** CV curves of the supernatant of the hybrid system grown autotrophically for 36 h under wave motion. The two controls are the supernatant of ZnO NSs only and *C. necator* only. **c** Midpoint potentials of the two redox couples (labeled as Redox 1 and 2) observed on the CV curve of the hybrid system's supernatant compared to biological components of *C. necator* involved in ET ($E^{\circ\prime}$: standard reduction potential at a physiological pH). **d** Flavin fluorescence spectra at 36 h of autotrophic growth in the supernatant of the biopiezocatalytic system compared to relevant controls. **e** Increase in flavin-related fluorescence in the supernatant of the piezo-stimulated hybrid system over time. **f** Protein models for the monoheme c-type cytochromes H16_A1121 (AFDB accession number AF-Q0KCK9-F1; https://alphafold.ebi.ac.uk/entry/Q0KCK9) and H16_A3570 (AFDB accession number AF-Q1LHT0-F1; https://alphafold.ebi.ac.uk/entry/Q1LHT0) detected in the supernatant of ZnO-*C. necator*[63]. Source data are provided as a Source Data file.

as H_2, which would then be oxidized by SH and MBH, or as e^- through flavins and extracellular cytochromes released by the microbial cells (Fig. 6). Through the activity of hydrogenases, H_2 from ZnO would augment the availability of intracellular reduced cofactors for PHB synthesis, CO_2 fixation, and oxidative phosphorylation. In the case of flavin/cytochrome-transferred e^-, because of the midpoint potentials of these carriers, they may mainly contribute to bioenergy generation via oxidative phosphorylation with corresponding protons possibly coming from h^+-triggered oxidation by ZnO[52]. At the moment, the relative importance in our system of the H_2-dependent and flavin/cytochrome-dependent ET mechanisms from ZnO to *C. necator* is unclear. The complete characterization of the full ET chain, including how extracellular flavins and cytochromes contribute precisely to charge transfer from ZnO NSs, as well as active bioenergy conservation mechanisms in the biopiezocatalytic system, warrants deeper investigations.

For heterotrophic growth and bioproduction from fructose by the ZnO-*C. necator* hybrid system, experimental evidence suggests a similar dual charge transfer mechanism. In the first route, H_2 produced by the piezocatalyst was likely oxidized by abundantly expressed SH and MBH (Supplementary Table 2). The heterotrophic ZnO-*C. necator* hybrid also released both flavins and the small c-type cytochromes H16_A1121 and H16_A3570 in the extracellular fraction, providing additional evidence supporting a function for these redox mediators in an alternative electron transfer route (Supplementary Figs. 20 and 21).

In summary, our finding indicates that a mechanically stimulated piezocatalyst can transfer charge to *C. necator* to increase bioplastic production. This hybrid system combines the capacity of ZnO to convert ubiquitous mechanical energy into electrochemical energy with the metabolic versatility of bacterial cells. We demonstrated that ZnO stimulates autotrophic PHB production, highlighting the potential of our approach for CO_2 bioconversion applications. We also showed that the same system promoted heterotrophic PHB synthesis from fructose by modulating the intracellular redox balance. Based on these results, autotrophic and heterotrophic biopiezocatalytic hybrids, such as the systems described here, could serve to improve and scale up integrated bioproduction by harnessing ubiquitous natural mechanical energy sources, including hydrological currents and waves. Furthermore, biopiezocatalytic hybrids can exploit widespread human-made vibrations from industrial installations to enhance bioprocesses. Biopiezocatalysts can also enable the recovery into final bioproducts of the electrical energy usually spent to agitate and aerate most industrial microbial processes.

In this study, we focused exclusively on ZnO NSs because of their extensively studied piezocatalytic properties. A subsequent avenue of research to tackle is how other types of ZnO with different piezoelectric coefficients, as well as other piezoresponsive minerals, polymers, metals, and perovskites[53] may interact with a microbial catalyst such as *C. necator*. A second route to explore is the engineering of *C. necator*, through available genetic tools[31], to better understand and improve its capacity to acquire charges from a piezocatalyst as well as develop other commercially-relevant bioproducts. A third aspect of the hybrid system that remains to be deciphered is how holes from mechanically stimulated ZnO NSs are scavenged. In addition to chemicals from the growth medium, bacteria such as *C. necator* produce thousands of metabolites. Future work will aim to determine which of these molecules could consume holes from ZnO NSs. By harnessing mechanical energy through a piezocatalyst, the hybrid system proposed here may help overcome productivity limitations that plague the development of autotrophic and heterotrophic biotechnologies. This is not limited to *C. necator*, and our approach can serve as a blueprint to drive bioproduction by a wide range of microbial platforms.

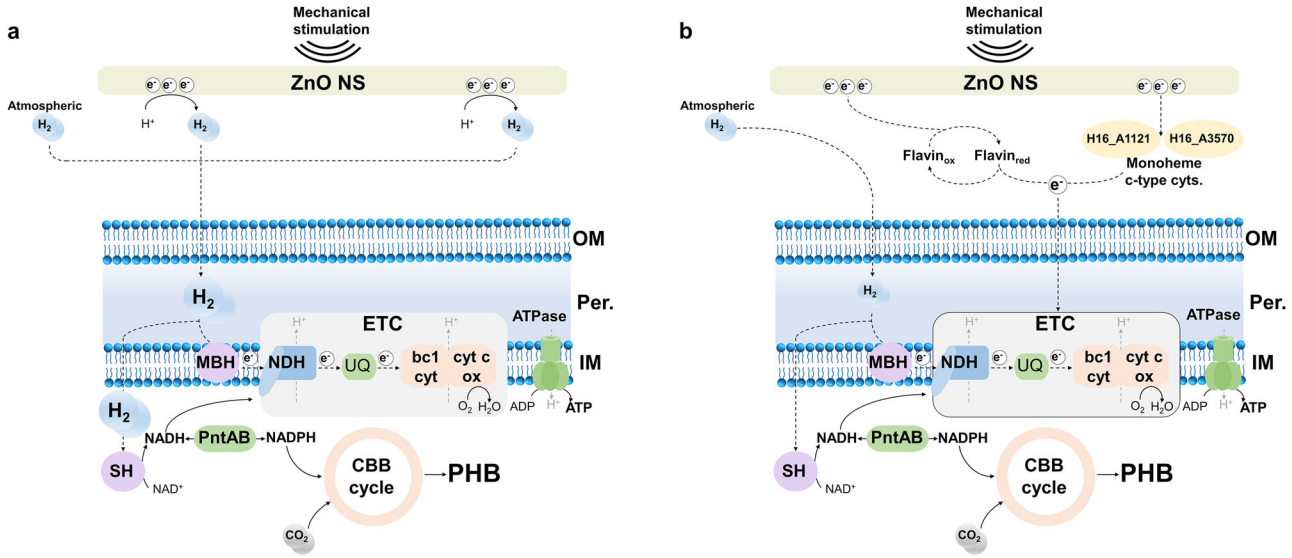

Fig. 6 | Proposed dual model of charge transfer mechanisms between ZnO and *C. necator* during piezo-stimulation under autotrophic growth conditions. a In the first mechanism, piezo-stimulated ZnO generates H_2, which, in addition to H_2 provided initially in the headspace, is oxidized by the hydrogenases of *C. necator*. **b** In the second possible mechanism, e^- are transferred to ET components of *C. necator*'s cell wall via flavins and c-type cytochromes released by the bacterium. Cn C. necator, Cyts cytochromes, OM outer membrane, Per periplasm, IM inner membrane, ETC electron transport chain SH soluble hydrogenase, MBH membrane-bound hydrogenase, NDH NADH dehydrogenase, UQ ubiquinone, bc1 cyt cytochrome bc1 complex, cyt c ox cytochrome c oxidase, PntAB transhydrogenase, CBB Calvin-Benson-Bassham cycle, PHB polyhydroxybutyrate.

Methods

ZnO nanosheets synthesis

ZnO NSs were synthesized hydrothermally by first dissolving 4 mmol of $Zn(NO_3)_2{\cdot}6H_2O$ in 30 mL of deionized water via continuous stirring for 15 min[54,55]. Separately, a second solution comprising 8 mmol of urea was prepared in 20 mL of deionized water. Both solutions were mixed by stirring, and the reaction was transferred to a Teflon-lined stainless-steel autoclave followed by incubation at 220 °C for 24 h. The resulting precipitate was cooled down to room temperature before being washed sequentially 3 times with deionized water and anhydrous ethanol to remove unreacted reagents and byproducts. Lastly, ZnO was dried under air in an oven at 60 °C, followed by a calcination step at 600 °C for 2 h.

Bacterial strain growth

The bacterium *C. necator* H16 (DSM 428) was acquired from the German Collection of Microorganisms and Cell Cultures (DSMZ). Unless stated otherwise, all *C. necator* cultures were grown at 30 °C in a nitrogen-limiting minimal (NLM) medium at pH 6.8 under mild agitation[56]. The NLM medium included 1 mL/L of trace element solution, 1 g/L NH_4Cl, 5.2 g/L $NaH_2PO_4{\cdot}2H_2O$, 11.6 g/L $Na_2HPO_4{\cdot}12H_2O$, 0.45 g/L K_2SO_4, 0.8 g/L $MgSO_4{\cdot}7H_2O$, and 0.08 g/L $CaCl_2{\cdot}2H_2O$. The trace element solution comprised 0.1 M HCl, 15 g/L $FeSO_4{\cdot}7H_2O$, 2.4 g/L $MnSO_4{\cdot}H_2O$, 2.4 g/L $ZnSO_4{\cdot}7H_2O$, and 0.48 g/L $CuSO_4.5H_2O$.

For autotrophic growth, *C. necator* was cultivated in 50 mL of NLM medium in a 250 mL serum bottle under a H_2:CO_2:O_2 atmosphere (74:13:13, 0.23 MPa). For heterotrophic growth, *C. necator* was cultivated in 50 mL of NLM medium including 20 g/L fructose under ambient atmosphere in a 250 mL flask. Bacterial growth was monitored by absorption spectrophotometry at an optical density of 600 nm ($OD_{600\ nm}$) with an Evolution 220 UV-vis spectrophotometer (Thermo Fisher Scientific, MA, USA).

Autotrophic and heterotrophic hybrid systems

To establish ZnO-*C. necator* hybrid systems, 0 to 1 g/L ZnO NSs was added to empty serum bottles or flasks, followed by sterilization by autoclaving. Where indicated, 0.8 g/L of amorphous SiO_2 (1000–2000 mesh) was added instead of ZnO NSs. Next, sterile NLM growth medium was poured into the serum bottles or flasks with ZnO NSs. For autotrophic experiments, a *C. necator* pre-culture grown without ZnO NSs was cultivated until reaching an $OD_{600\ nm}$ of ca. 1.0. Next, a 5 % (v/v) inoculum from this pre-culture was transferred to NLM medium with different concentrations of ZnO NSs. The serum bottle containing the hybrid system was then pressurized with H_2:CO_2:O_2 under sterile conditions. A similar procedure was employed for heterotrophic experiments, with the exception of the gas pressurization step, which was omitted. Where indicated, ZnO-*C. necator* NSs biopiezocatalytic hybrids and relevant controls were submitted to US in a KS-100DE ultrasonicator bath (40 Hz, Kunshan Jielimei Ultrasonic Instrument, China) for 1 h per day at 0 to 120 W to stimulate the ZnO NSs piezocatalyst. In a different assay, the cultures were grown under intense tilting agitation at 200 rpm (wave motion) instead of milder orbital shaking at 100 rpm.

For autotrophic experiments, all the different control and experimental groups were cultivated in 50 mL of NLM in a 250 mL serum bottle pressurized with H_2:CO_2:O_2 at a ratio of 74:13:13 at 0.23 MPa. Unless stated otherwise, cultures were agitated at 100 rpm. The controls were *C. necator* grown alone (Cn), *C. necator* grown alone and submitted daily to US (usually at 96 W for 1 h per day), *C. necator* grown with ZnO NSs (usually 0.8 g/L) (Cn/ZnO), and *C. necator* grown under intense tilting agitation at 200 rpm (Cn/wave). The experimental groups were *C. necator* submitted daily to US grown with ZnO NSs (Cn/ZnO/US) and *C. necator* under intense tilting agitation at 200 rpm grown with ZnO NSs (Cn/ZnO/wave). For heterotrophic experiments, the same control and experimental groups were cultivated. The notable differences were that *C. necator* was grown in NLM with 20 g/L of fructose under air at standard atmospheric pressure and that the usual concentration of ZnO NSs was 0.5 g/L.

For PHB measurement by acidified methanolysis[57], 5 mL samples were taken at different time points from bacterial cultures and centrifuged at 8000 × *g* for 5 min at 4 °C. Pellets were washed twice with deionized water before being dried overnight at 55 °C. Dried samples were reacted for 4 h at 100 °C in an acidified methanol solution comprising 1.94 mL methanol, 0.06 mL H_2SO_4, and 2 mL chloroform. Next,

1 mL of deionized water was added to each reaction, followed by vigorous mixing. Extracted PHB, in the form of 3-hydroxybutyrate methyl ester (HBME), was quantified with a GC9720 gas chromatograph (Fuli, Zhejiang, China) equipped with a DB-FFAP column and a flame ionization detector[32]. The M_w and PDI of the PHB produced by our system were determined with a PL-GPC50 gel permeation chromatography system (Agilent, CA, USA). The PDI was calculated with Eq. 1:

$$\mathrm{PDI} = M_w / M_n \quad (1)$$

Where M_n corresponds to the number average molecular weight.

Fructose consumption was measured by high-performance liquid chromatography, after filtering the samples with 0.22 µm filters, with a Breeze 2 system (Waters, MA, USA) equipped with an Aminex HPX-87H anion exchange column (Bio-Rad, CA, USA)[32]. Soluble protein concentrations were measured in whole-cell lysates with a bicinchoninic assay kit (Sparkjade, Qingdao, China).

^{13}C-bicarbonate labelling assay

The ^{13}C-tracer experiment was conducted with several modifications[58]. ^{13}C-bicarbonate (98%, Shanghai yuanye Bio-Technology, China) (12.5% of total HCO_3^-/CO_2 in serum bottles) was added at time 0 to *C. necator* hybrid systems cultivated with 0.8 g/L ZnO NSs grown under autotrophic conditions. After 36 h, 10 mL of culture was centrifuged at 8000 × *g* for 5 min at 4 °C. After washing and drying, PHB was extracted from *C. necator* cells by acidified methanolysis. The organic phase from this process, which contains HBME derived from PHB, was analyzed by gas chromatography-mass spectrometry (GC-MS) with a 6890N/5975 system (Agilent, CA, USA). Distinctive GC-MS peaks for HBME were detected at *m/z* 43 (M + 0), and 44 (M + 1), and the ^{13}C and ^{12}C isotope fractions were calculated[59].

Characterization of ZnO and ZnO-*C. necator* aggregates

X-ray diffraction spectroscopy of ZnO NSs was completed with a D8 ADVANCE system (Bruker, MA, USA) in the 10° to 80° range with Cu Kα radiation. X-ray photoelectron spectroscopy was done with an ESCALAB Xi+ spectrometer using monochromatic Al Kα radiation (Thermo Fisher Scientific). UV-vis DRS was completed with a Lambda 750S spectrophotometer (PerkinElmer, MA, USA) within a wavelength range of 200–800 nm. SEM micrographs of ZnO NSs, *C. necator*, and the ZnO-*C. necator* hybrid system were taken with a S-4800 microscope (Hitachi, Japan) at a 5 kV accelerating voltage. The same apparatus was employed to acquire EDS maps. For SEM and EDS, the hybrid system samples came from an intensely agitated (200 rpm, tilting shaker) ZnO-*C. necator* autotrophic culture after 24 h of growth. Samples were preserved in 0.1 M Na phosphate buffer (pH 7.0) with 2.5% glutaraldehyde, dehydrated with ethanol gradient, and air dried on a silicon wafer before SEM examination. The PFM analysis of the hybrid system was performed with a MFP-3D AFM (Oxford Instruments, UK). Hydrodynamic particle sizes were measured by dynamic light scattering with a Zetasizer Nano ZS90 size analyzer (Malvern Panalytical, UK).

Live/dead staining of autotrophic and heterotrophic hybrid systems was completed by staining microbial populations with the SYTO 9 green fluorescent dye and propidium iodide. The samples were then examined with an Eclipse Ti2 inverted microscope (Nikon, Japan). Before staining, bacterial cultures were diluted 10 to 100-fold. In this assay, cells stained in green are considered alive, while cells stained in red have compromised membranes and are considered dead.

Electrochemical characterization and photoluminescence

All electrochemical experiments were carried out with a three-electrode system and a CHI600E potentiostat (CH Instruments, TX, USA). A Pt sheet (1 cm^2) was the counter electrode, and an Ag/AgCl electrode (3.5 M KCl) was the reference. For EIS, the working electrode (WE) was glassy carbon (*d* = 3 mm) and the electrolyte was sterile NLM medium. EIS data for both ZnO and the ZnO-*C. necator* hybrid grown autotrophically were acquired with a sinusoidal voltage of 5 mV within frequencies ranging from 100 kHz to 0.1 Hz with a 0.3 V bias. For the transient piezoelectric current experiment, 10 mg of the autotrophic ZnO-*C. necator* hybrid or ZnO NSs only was suspended in a 5% (v/v) Nafion solution (DuPont, DE, USA) and coated on a fluorine-doped tin oxide (FTO) (4 cm^2) WE. Transient piezoelectric current was measured with an on/off US cycle at 96 W for a total time of 300 s and a bias of 0.3 V. The Mott–Schottky analysis of ZnO NSs was completed with a FTO WE. 10 mg of ZnO NSs was suspended in a Nafion solution, and this mixture was deposited uniformly on the FTO WE, which was then dried for 4 h at 55 °C. The Mott–Schottky analysis was performed from −1.0 V to 0 V with a frequency of 10 Hz. CV of the autotrophic hybrid system's supernatant was done with a glassy carbon WE and a scan rate of 10 mV/s. Prior to the experiment, supernatants for the different groups grown for 24 h were collected by centrifugation, followed by flushing with pure N_2 for 15 min. PL spectra were recorded at an excitation wavelength of 315 nm with a F-7000 fluorescence spectrophotometer (Hitachi, Japan).

Electronic band structure of ZnO nanosheets

The ZnO NSs band gap energy (E_g) of 3.2 eV was calculated with the Tauc plots derived from UV-vis DRS data. The Mott–Schottky plot exhibited a positive slope, which is expected for n-type ZnO[60], as well as a flat-band potential (E_{fb}) of −0.63 V (vs Ag/AgCl). After conversion to the standard hydrogen electrode (SHE) potential, the E_{fb} was −0.43 V. In n-type semiconductors, the conduction band edge (E_{cb}) is more negative than the E_{fb} by ca. 0.1 to 0.2 V[61]. Consequently, the E_{cb} was estimated to be −0.53 V vs SHE. The valence band edge (E_{vb}) was calculated with Eq. 2:

$$E_g = E_{vb} - E_{cb} \quad (2)$$

Based on this equation, the E_{vb} was 2.67 V.

Intracellular NADPH/NADP$^+$ ratio, extracellular flavin, and c-type cytochrome analyses

Intracellular NADPH/NADP$^+$ ratios were measured after 36 h of autotrophic growth or 96 h of heterotrophic growth. At these time points, *C. necator* cell samples were snap-frozen with liquid nitrogen to stop the metabolism. Next, the samples were thawed, and NADPH/NADP$^+$ ratios were measured with the coenzyme II NADP(H) content assay kit (Solarbio, Beijing, China). For flavin detection in the hybrid system's supernatant, 3 mL of culture was centrifuged at 8000 × *g* for 5 min at 4 °C. Emission spectra of the supernatant from different samples were measured with a F-7000 fluorescence spectrophotometer (Hitachi) at an excitation wavelength of 425 nm. In the presence of flavin, a peak is expected to be detected at ca. 525 nm[48].

For the c-type cytochromes analysis, autotrophic and heterotrophic cultures under tilting agitation at 200 rpm were grown for 36 h. Supernatants were collected by centrifugation at 8000 × *g* for 10 min at 4 °C before being concentrated 25 times with Amicon ultra-15 centrifugal filter units with a nominal M_w limit of 3 kDa (Sigma-Aldrich, MA, USA). Concentrated supernatant samples were then loaded on a SDS-PAGE gel for protein separation, followed by heme staining[62]. Next, gel bands of interest were excised and analyzed by liquid chromatography coupled with tandem MS (Sangon, Shanghai, China). The structures of the c-type cytochromes H16_A1121 and H16_A3570 and the location of the heme cofactors were predicted with AlphaFold3[63].

H_2 evolution by ZnO incubated in cell-free spent medium

For this experiment, cell-free spent medium was obtained from both autotrophic and heterotrophic ZnO-*C. necator* hybrid systems. First, hybrid cultures were grown for 24 h before collecting cell-free

supernatants by centrifugation at 8000 × *g* for 5 min at 4 °C. 20 mL of cell-free spent medium was then transferred to a 120 mL serum bottle, followed by the addition of 10 mg of ZnO NSs. This approach was adopted to recreate conditions, through the usage of cell-free spent medium, close to an active microbial culture but without cells oxidizing H_2, which would interfere with H_2 measurement. Next, the serum bottle was capped and flushed for 15 min with N_2 gas. Piezocatalytic ZnO NSs were submitted to US for 1 h at 96 W, and H_2 was measured with a GC9720 Plus gas chromatograph (FULI, China).

Transcriptomic and quantitative PCR analyses

For transcriptomic analyses, *C. necator* was grown autotrophically in triplicate with 0.8 g/L ZnO NSs under intense tilting agitation at 200 rpm. After 36 h, bacterial cells were collected by centrifugation at 8000 × *g* for 5 min at 4 °C and washed twice with phosphate-buffered saline (PBS). The samples were then re-suspended in PBS and snap-frozen in liquid nitrogen. Next, total RNA was extracted with the TRIzol reagent (Thermo Fisher Scientific). The RNA sequencing library was prepared with the VAHTS™ Stranded mRNA-seq V2 Library Prep Kit (Vazyme, Jiangsu, China). Paired-end RNA sequencing with an average read length of 150 nt was completed with a DNBSEQ-T7 sequencing instrument (MGI, Guangdong, China). Reads were mapped to the reference genome GCA_000009285.2 of *C. necator* H16 with Bowtie 2[64]. The featureCounts program was then employed to normalize mapped reads with the transcripts per million (TPM) method[65].

For quantitative PCR (qPCR) done to study the expression of SH (PHG088, *hoxF*) and MBH (PHG001, *hoxK*) in heterotrophic hybrid systems, *C. necator* cells grown with mechanically-stimulated ZnO NSs were collected after 36 h of growth. Total RNA was extracted with the RNApure Bacteria Kit (CWBio, Taizhou, China), followed by conversion into cDNA with SPARKscript II (Sparkjade). The qPCR experiment was completed with the Sybr Green M5 HiPer Realtime PCR Super Mix (Mei5bio, Beijing, China) and a CFX Connect Real-Time PCR Detection device (Bio-Rad). The expression of *hoxF* and *hoxK* was compared to the housekeeping gene *gyrB* (H16_A0003)[66]. Primers used for qPCR are listed in Supplementary Table 3.

Statistics and reproducibility

All experiments were biologically repeated independently three times. This includes micrographs presented in Fig. 1c-e, and Supplementary Figs. 3, 4, 9, and 13. Results are considered to be statistically significant when the *p* value calculated with the two-tailed paired Student's *t*-test is below or equal to 0.05.

Reporting summary

Further information on research design is available in the Nature Portfolio Reporting Summary linked to this article.

Data availability

Data generated in this study are provided within the paper and its Supplementary information. Datasets for RNA sequencing are available in the NCBI GEO database under accession number GSE283974. Source data are provided with this paper.

References

1. Tilsted, J. P., Bauer, F., Birkbeck, C. D., Skovgaard, J. & Rootzén, J. Ending fossil-based growth: confronting the political economy of petrochemical plastics. *One Earth* **6**, 607–619 (2023).
2. Bachleitner, S., Ata, Ö & Mattanovich, D. The potential of CO_2-based production cycles in biotechnology to fight the climate crisis. *Nat. Commun.* **14**, 6978 (2023).
3. Liew, F. E. et al. Carbon-negative production of acetone and isopropanol by gas fermentation at industrial pilot scale. *Nat. Biotechnol.* **40**, 335–344 (2022).
4. Jiang, W. et al. Metabolic engineering strategies to enable microbial utilization of C1 feedstocks. *Nat. Chem. Biol.* **17**, 845–855 (2021).
5. Lv, X. et al. C1-based biomanufacturing: advances, challenges and perspectives. *Bioresour. Technol.* **367**, 128259 (2023).
6. Rial, R. C. Biofuels versus climate change: exploring potentials and challenges in the energy transition. *Renew. Sustain. Energy Rev.* **196**, 114369 (2024).
7. Bae, J., Jin, S., Kang, S., Cho, B.-K. & Oh, M.-K. Recent progress in the engineering of C1-utilizing microbes. *Curr. Opin. Biotechnol.* **78**, 102836 (2022).
8. Zhang, T. & Tremblay, P.-L. Hybrid photosynthesis-powering biocatalysts with solar energy captured by inorganic devices. *Biotechnol. Biofuels* **10**, 249 (2017).
9. Blankenship, R. E. et al. Comparing photosynthetic and photovoltaic efficiencies and recognizing the potential for improvement. *Science* **332**, 805–809 (2011).
10. Tremblay, P.-L., Xu, M., Chen, Y. & Zhang, T. Nonmetallic abiotic-biological hybrid photocatalyst for visible water splitting and carbon dioxide reduction. *iScience* **23**, 100784 (2020).
11. Kuang, M. et al. Carbon dioxide upgrading to biodegradable plastics through photo/electro-synthetic biohybrid systems. *Angew. Chem. Int. Ed.* https://doi.org/10.1002/anie.202422357 (2024).
12. Zhang, T. More efficient together. *Science* **350**, 738–739 (2015).
13. Jiang, Y., Li, H. & Zhu, W. Single-bacterium modification strategies for photobiocatalytic CO_2 reduction. *Trends Chem.* **6**, 577–580 (2024).
14. Ye, J. et al. Solar-driven methanogenesis with ultrahigh selectivity by turning down H_2 production at biotic-abiotic interface. *Nat. Commun.* **13**, 6612 (2022).
15. Cestellos-Blanco, S., Zhang, H., Kim, J. M., Shen, Y. & Yang, P. Photosynthetic semiconductor biohybrids for solar-driven biocatalysis. *Nat. Catal.* **3**, 245–255 (2020).
16. Curie, J. & Curie, P. Développement par compression de l'électricité polaire dans les cristaux hémièdres à faces inclinées. *Bull. Minéral.* **3**, 90–93 (1880).
17. Wang, K. et al. The mechanism of piezocatalysis: Energy band theory or screening charge effect? *Angew. Chem. Int. Ed.* **61**, e202110429 (2022).
18. Tu, S. et al. Piezocatalysis and piezo-photocatalysis: catalysts classification and modification strategy, reaction mechanism, and practical application. *Adv. Funct. Mater.* **30**, 2005158 (2020).
19. Liang, Z., Yan, C.-F., Rtimi, S. & Bandara, J. Piezoelectric materials for catalytic/photocatalytic removal of pollutants: recent advances and outlook. *Appl. Catal. B Environ.* **241**, 256–269 (2019).
20. Starr, M. B., Shi, J. & Wang, X. Piezopotential-driven redox reactions at the surface of piezoelectric materials. *Angew. Chem. Int. Ed.* **51**, 5962–5966 (2012).
21. Zheng, H. et al. Recent advancements in the use of novel piezoelectric materials for piezocatalytic and piezo-photocatalytic applications. *Appl. Catal. B Environ.* **341**, 123335 (2024).
22. Cao, X. et al. Piezoelectric nanogenerators derived self-powered sensors for multifunctional applications and artificial intelligence. *Adv. Funct. Mater.* **31**, 2102983 (2021).
23. Chen, S. et al. Piezocatalytic medicine: an emerging frontier using piezoelectric materials for biomedical applications. *Adv. Mater.* **35**, 2208256 (2023).
24. Ye, J. et al. Wastewater denitrification driven by mechanical energy through cellular piezo-sensitization. *Nat. Water* **2**, 531–540 (2024).
25. Ren, G. et al. Mechanical energy drives the growth and carbon fixation of electroactive microorganisms. *Engineering* https://doi.org/10.1016/j.eng.2024.08.006 (2024).
26. Wang, Z. L. & Song, J. Piezoelectric nanogenerators based on zinc oxide nanowire arrays. *Science* **312**, 242–246 (2006).

27. Xiong, X. et al. Oxygen vacancy engineering of zinc oxide for boosting piezo-electrocatalytic hydrogen evolution. *Appl. Surf. Sci.* **616**, 156556 (2023).
28. Wang, B. et al. Co-catalyst-free large ZnO single crystal for high-efficiency piezocatalytic hydrogen evolution from pure water. *J. Energy Chem.* **65**, 304–311 (2022).
29. Le, A. T., Ahmadipour, M. & Pung, S.-Y. A review on ZnO-based piezoelectric nanogenerators: synthesis, characterization techniques, performance enhancement and applications. *J. Alloy. Compd.* **844**, 156172 (2020).
30. Lee, J., Park, H. J., Moon, M., Lee, J.-S. & Min, K. Recent progress and challenges in microbial polyhydroxybutyrate (PHB) production from CO_2 as a sustainable feedstock: a state-of-the-art review. *Bioresour. Technol.* **339**, 125616 (2021).
31. Morlino, M. S. et al. *Cupriavidus necator* as a platform for polyhydroxyalkanoate production: an overview of strains, metabolism, and modeling approaches. *Biotechnol. Adv.* **69**, 108264 (2023).
32. Xu, M., Tremblay, P.-L., Jiang, L. & Zhang, T. Stimulating bioplastic production with light energy by coupling *Ralstonia eutropha* with the photocatalyst graphitic carbon nitride. *Green. Chem.* **21**, 2392–2400 (2019).
33. Yeo, J. C. C., Muiruri, J. K., Thitsartarn, W., Li, Z. & He, C. Recent advances in the development of biodegradable PHB-based toughening materials: approaches, advantages and applications. *Mater. Sci. Eng. C.* **92**, 1092–1116 (2018).
34. Arikawa, H., Sato, S., Fujiki, T. & Matsumoto, K. A study on the relation between poly(3-hydroxybutyrate) depolymerases or oligomer hydrolases and molecular weight of polyhydroxyalkanoates accumulating in *Cupriavidus necator* H16. *J. Biotechnol.* **227**, 94–102 (2016).
35. Liu, J., Zhang, H., Jiang, X., Tremblay, P.-L. & Zhang, T. An efficient and reusable N,N-dimethylacetamide/LiCl solvent system for the extraction of high-purity polyhydroxybutyrate from bacterial biomass. *Biochem. Eng. J.* **192**, 108812 (2023).
36. Xu, M. et al. Photo-augmented PHB production from CO_2 or fructose by *Cupriavidus necator* and shape-optimized CdS nanorods. *Sci. Total Environ.* **753**, 142050 (2021).
37. Slater, S. C., Voige, W. H. & Dennis, D. E. Cloning and expression in *Escherichia coli* of the *Alcaligenes eutrophus* H16 poly-beta-hydroxybutyrate biosynthetic pathway. *J. Bacteriol.* **170**, 4431–4436 (1988).
38. Sirelkhatim, A. et al. Review on zinc oxide nanoparticles: antibacterial activity and toxicity mechanism. *Nano-Micro Lett.* **7**, 219–242 (2015).
39. Kumar, R., Umar, A., Kumar, G. & Nalwa, H. S. Antimicrobial properties of ZnO nanomaterials: a review. *Ceram. Int.* **43**, 3940–3961 (2017).
40. Pohlmann, A. et al. Genome sequence of the bioplastic-producing "Knallgas" bacterium *Ralstonia eutropha* H16. *Nat. Biotechnol.* **24**, 1257–1262 (2006).
41. Hossain, S. T. & Mukherjee, S. K. Toxicity of cadmium sulfide (CdS) nanoparticles against *Escherichia coli* and HeLa cells. *J. Hazard. Mater.* **260**, 1073–1082 (2013).
42. Jiang, Y., Yang, X., Zeng, D., Su, Y. & Zhang, Y. Microbial conversion of syngas to single cell protein: the role of carbon monoxide. *Chem. Eng. J.* **450**, 138041 (2022).
43. Wang, J., Xu, M., Tremblay, P.-L. & Zhang, T. Improved polyhydroxybutyrate production by *Cupriavidus necator* and the photocatalyst graphitic carbon nitride from fructose under low light intensity. *Int. J. Biol. Macromol.* **203**, 526–534 (2022).
44. Cramm, R. Genomic view of energy metabolism in *Ralstonia eutropha* H16. *J. Mol. Microbiol. Biotechnol.* **16**, 38–52 (2008).
45. Li, H. et al. Integrated electromicrobial conversion of CO_2 to higher alcohols. *Science* **335**, 1596–1596 (2012).
46. Fu, B. et al. Single-cell multimodal imaging uncovers energy conversion pathways in biohybrids. *Nat. Chem.* **15**, 1400–1407 (2023).
47. Stewart, R. C. & Massey, V. Potentiometric studies of native and flavin-substituted Old Yellow Enzyme. *J. Biol. Chem.* **260**, 13639–13647 (1985).
48. Okamoto, A. et al. Uptake of self-secreted flavins as bound cofactors for extracellular electron transfer in Geobacter species. *Energy Environ. Sci.* **7**, 1357–1361 (2014).
49. Kömen, R., Zannoni, D., Ingledew, W. J. & Schmidt, K. The electron transport system of *Alcaligenes eutrophus* H16. *Arch. Microbiol.* **155**, 382–390 (1991).
50. Lovley, D. R. & Holmes, D. E. Electromicrobiology: the ecophysiology of phylogenetically diverse electroactive microorganisms. *Nat. Rev. Microbiol.* **20**, 5–19 (2022).
51. Fernandes, T. M., Silva, M. A., Morgado, L. & Salgueiro, C. A. Hemes on a string: insights on the functional mechanisms of PgcA from Geobacter sulfurreducens. *J. Biol. Chem.* **299**, 105167 (2023).
52. Ning, X., Hao, A., Chen, R., Khan, M. F. & Jia, D. Constructing of GQDs/ZnO S-scheme heterojunction as efficient piezocatalyst for environmental remediation and understanding the charge transfer mechanism. *Carbon* **218**, 118772 (2024).
53. Jia, P., Li, J. & Huang, H. Piezocatalysts and piezo-photocatalysts: From material design to diverse applications. *Adv. Funct. Mater.* **34**, 2407309 (2024).
54. Van Duy, L. et al. Ultrasensitive NO_2 gas sensing performance of two dimensional ZnO nanomaterials: Nanosheets and nanoplates. *Ceram. Int.* **47**, 28811–28820 (2021).
55. Li, S.-M. et al. Acetone sensing of ZnO nanosheets synthesized using room-temperature precipitation. *Sens. Actuators B Chem.* **249**, 611–623 (2017).
56. Budde, C. F., Mahan, A. E., Lu, J., Rha, C. & Sinskey, A. J. Roles of multiple acetoacetyl coenzyme A reductases in polyhydroxybutyrate biosynthesis in *Ralstonia eutropha* H16. *J. Bacteriol.* **192**, 5319–5328 (2010).
57. Braunegg, G., Sonnleitner, B. & Lafferty, R. M. A rapid gas chromatographic method for the determination of poly-β-hydroxybutyric acid in microbial biomass. *Eur. J. Appl. Microbiol. Biotechnol.* **6**, 29–37 (1978).
58. Pham, D. N., Mai, D. H. A. & Lee, E. Y. Biosynthesis of polyhydroxybutyrate from methane and carbon dioxide using type II methanotrophs. *Bioresour. Technol.* **405**, 130931 (2024).
59. Jennings, M. E. & Matthews, D. E. Determination of complex isotopomer patterns in isotopically labeled compounds by mass spectrometry. *Anal. Chem.* **77**, 6435–6444 (2005).
60. Li, H., Liu, J., Wang, C., Yang, H. & Xue, X. Oxygen vacancies-enriched and porous hierarchical structures of ZnO microspheres with improved photocatalytic performance. *Vacuum* **199**, 110891 (2022).
61. Liu, Z., Liu, X., Yu, C., Wei, L. & Ji, H. Fabrication and characterization of I doped Bi_2MoO_6 microspheres with distinct performance for removing antibiotics and Cr(VI) under visible light illumination. *Sep. Purif. Technol.* **247**, 116951 (2020).
62. Thomas, P. E., Ryan, D. & Levin, W. An improved staining procedure for the detection of the peroxidase activity of cytochrome *P*-450 on sodium dodecyl sulfate polyacrylamide gels. *Anal. Biochem.* **75**, 168–176 (1976).
63. Abramson, J. et al. Accurate structure prediction of biomolecular interactions with AlphaFold 3. *Nature* **630**, 493–500 (2024).
64. Langmead, B. & Salzberg, S. L. Fast gapped-read alignment with Bowtie 2. *Nat. Methods* **9**, 357–359 (2012).
65. Liao, Y., Smyth, G. K. & Shi, W. featureCounts: an efficient general purpose program for assigning sequence reads to genomic features. *Bioinformatics* **30**, 923–930 (2014).
66. Jugder, B.-E. et al. An analysis of the changes in soluble hydrogenase and global gene expression in *Cupriavidus necator*

(*Ralstonia eutropha*) H16 grown in heterotrophic diauxic batch culture. *Microb. Cell Factor.* **14**, 42 (2015).

Acknowledgements

This project was funded by the National Natural Science Foundation of China (No 42272355) (T.Z.) and the Hainan Yazhou Bay Science and Technology Bureau (No SKJC-2020-01-004) (T.Z.).

Author contributions

P.-L.T. and T.Z. designed the study. M.X., M.B.J. and L.L. prepared the piezocatalyst and performed the PHB and soluble protein production experiments. M.X. and M.B.J. characterized the biopiezocatalytic system. Y.W. and C.H. completed the microscopy, electrochemical, and biochemical analyses. Z.L. did the transcriptomic, qPCR, and protein biochemisty experiments. K.X. and Y.F. completed and analyzed the ^{13}C-bicarbonate labelling assay. P.-L.T., M.X. and T.Z. analyzed the data and prepared the figures. P.-L.T. wrote the original draft. P.-L.T., Y.F. and T.Z. reviewed and revised the manuscript. T.Z. acquired the funding and supervised the study. All authors approved the final manuscript.

Competing interests

The authors declare no competing interests.

Additional information

Supplementary information The online version contains supplementary material available at https://doi.org/10.1038/s41467-025-63576-y.

Correspondence and requests for materials should be addressed to Tian Zhang.

Peer review information *Nature Communications* thanks Jiazhang Lian, and the other, anonymous, reviewer(s) for their contribution to the peer review of this work. A peer review file is available.

Reprints and permissions information is available at http://www.nature.com/reprints

Publisher's note Springer Nature remains neutral with regard to jurisdictional claims in published maps and institutional affiliations.

Open Access This article is licensed under a Creative Commons Attribution-NonCommercial-NoDerivatives 4.0 International License, which permits any non-commercial use, sharing, distribution and reproduction in any medium or format, as long as you give appropriate credit to the original author(s) and the source, provide a link to the Creative Commons licence, and indicate if you modified the licensed material. You do not have permission under this licence to share adapted material derived from this article or parts of it. The images or other third party material in this article are included in the article's Creative Commons licence, unless indicated otherwise in a credit line to the material. If material is not included in the article's Creative Commons licence and your intended use is not permitted by statutory regulation or exceeds the permitted use, you will need to obtain permission directly from the copyright holder. To view a copy of this licence, visit http://creativecommons.org/licenses/by-nc-nd/4.0/.

© The Author(s) 2025